JACS
JOURNAL OF THE AMERICAN CHEMICAL SOCIETY
Article
pubs.acs.org/JACS

Embedding Covalency into Metal Catalysts for Efficient Electrochemical Conversion of CO_2

Hyung-Kyu Lim,[§,†] Hyeyoung Shin,[§,†] William A. Goddard, III,[‡] Yun Jeong Hwang,[∥] Byoung Koun Min,[∥,⊥] and Hyungjun Kim*[,†]

[†]Graduate School of Energy, Environment, Water, and Sustainability (EEWS), Korea Advanced Institute of Science and Technology (KAIST), Yuseong-gu, Daejeon 305-701, Korea

[‡]Materials and Process Simulation Center, Beckman Institute, California Institute of Technology, Pasadena, California 91125, United States

[∥]Clean Energy Research Center, Korea Institute of Science and Technology (KIST), Seongbuk-gu, Seoul 136-791, Korea

[⊥]Green School, Korea University, Seongbuk-gu, Seoul 136-713, Korea

Supporting Information

ABSTRACT: CO_2 conversion is an essential technology to develop a sustainable carbon economy for the present and the future. Many studies have focused extensively on the electrochemical conversion of CO_2 into various useful chemicals. However, there is not yet a solution of sufficiently high enough efficiency and stability to demonstrate practical applicability. In this work, we use first-principles-based high-throughput screening to propose silver-based catalysts for efficient electrochemical reduction of CO_2 to CO while decreasing the overpotential by 0.4−0.5 V. We discovered the covalency-aided electrochemical reaction (CAER) mechanism in which *p*-block dopants have a major effect on the modulating reaction energetics by imposing partial covalency into the metal catalysts, thereby enhancing their catalytic activity well beyond modulations arising from *d-block* dopants. In particular, sulfur or arsenic doping can effectively minimize the overpotential with good structural and electrochemical stability. We expect this work to provide useful insights to guide the development of a feasible strategy to overcome the limitations of current technology for electrochemical CO_2 conversion.

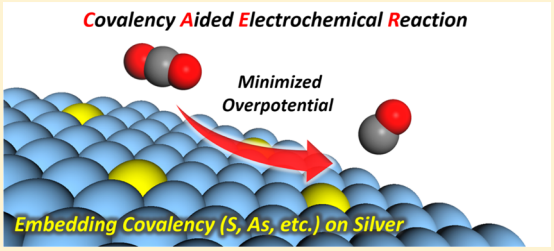

INTRODUCTION

For the mitigation of global-warming problems and the sustainable development of the inevitable carbon-based economy, carbon dioxide (CO_2) conversion technology has been regarded as one of the most important and urgent current scientific issues. Many researchers anticipate the efficient transformation of CO_2 from various emission sources into more valuable chemicals and fuels. Among the various ongoing attempts, which are categorized as biochemical, thermochemical, electrochemical, and photoassisted electrochemical processes,[1] the electrochemical method has certain merits in terms of high reactivity at ambient conditions and good extensibility from small to large-scale processes.[2] The possibility of direct integration with renewable electric sources adds more potential to the electrochemical method as a promising route for CO_2 conversion.

To bring electrochemical CO_2 conversion technology into practice, it requires significant improvements in (1) energetic efficiencies, (2) catalytic stability, and (3) current density.[3] A current bottleneck discouraging the practical application of electrochemical CO_2 conversion is mostly derived from the high thermodynamic barrier of the CO_2-to-CO_2^- electron uptake process. Because this process accompanies the disruption of the stable sp-hybridization symmetry on the carbon atom to bend the linear molecule,[4] it requires a substantial energy (−1.9 V vs SHE in a dimethylformamide solution).[5] Thus, it is critical to develop catalysts facilitating electron transfer to CO_2 and properly stabilizing an intermediate species to reduce the overpotential for the entire electrochemical process.[6,7]

The search for and development of new materials and catalysts are now being accelerated by computational simulations due to recent advances in materials-simulation methods, both in the form of enhanced accuracy and reduced computational times. Simulation-guided rational design of materials and catalysts, termed in-silico design, has been a long-standing dream of theorists and is becoming an inevitable and cost-effective materials-development process.[8] For instance, high-throughput screening of materials using computational simulations is being actively used and has yielded great improvements in materials properties for applications such as secondary battery electrodes,[9−11] fuel cell catalysts,[12] photo-

Received: April 15, 2014
Published: July 25, 2014

   dx.doi.org/10.1021/ja503782w | J. Am. Chem. Soc. 2014, 136, 11355−11361

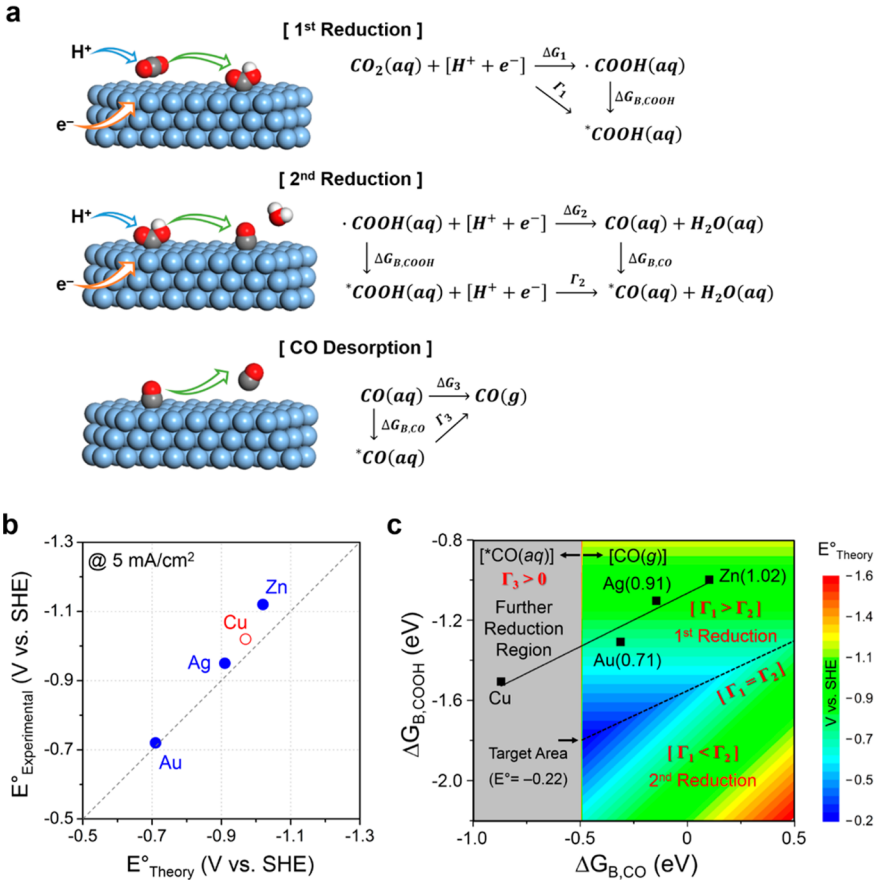

Figure 1. Thermodynamic and quantum-mechanical aspects of the CO_2-to-CO reduction process. (a) Schematic representation and the Born–Haber cycle for elementary reaction pathways from CO_2 to CO. (b) Comparison between the theoretical and the experimental reduction potential of Zn, Ag, Au, and Cu. The overpotentials for Zn, Ag, and Au originate from the first reduction process, whereas that for Cu originates from the third reduction process (Supporting Information Table S2). (c) 2D contour map of the theoretical reduction potential in terms of the solvated binding free energies of ·COOH and CO on the catalyst surface. The theoretical minimum bound of the reduction potential is −0.22 V vs SHE, which is shifted from the linear correlation for pure metal catalysts.

voltaics,[13] metal organic frameworks (MOF) for gas storage,[14] and so forth.

In this study, we therefore performed the in-silico design of metal catalysts to develop efficient electrochemical CO_2-conversion catalysts. Toward this goal, we first carefully investigated the electrochemical CO_2-reduction mechanism, enabling accurate and quantitative predictions of the reduction potentials from first-principles-based calculations coupled with the Poisson–Boltzmann (PB) implicit solvation method. Then, we performed high-throughput screening of atomic-level dopants to maximize the catalytic activity, for which the covalency embedded in a metal by the introduction of the *p*-block dopant results in the selective stabilization of the intermediate species without stabilizing the final product, leading to a minimized overpotential.

METHODS

Density functional theory (DFT) calculations were performed using the Vienna Ab-initio Software Package (VASP).[15] All calculations were carried out with the Perdew–Burke–Ernzerhof (PBE) exchange-correlation functional,[16] and the electron–ion interaction was considered in the form of the projector-augmented-wave (PAW) method with a plane wave up to an energy of 600 eV. The (4 × 4) periodic slab models with three atomic layers combined with a 20 Å vacuum layer along the *z* axis were generated after fully minimizing the bulk crystal structure with a Monkhorst *k*-point grid of (18 × 18 × 18). The closest-packed faces, which are (111) for the FCC structure (for Cu, Ag, and Au) and (0001) for the HCP structure (for Zn) were considered to be representative reactive surfaces and the (5 × 5 × 1) *k*-point grid was employed. Additionally, a dipole correction was applied to all cases along the *z* direction, and one bottom layer was fixed during the geometry-optimization processes, whereas the upper two layers were allowed to relax. For a simpler screening calculation, only the plane-wave cutoff energy was reduced by 25%. The molecular vibrational terms were calculated for each optimized structure and converted into the vibrational internal energy and entropy for the condition of disregarding the vibrational temperature under 100 K. To estimate the enthalpy changes during solvation process, the Poisson–Boltzmann (PB) implicit solvation model, implemented in the VASP program[17] was employed using a dielectric constant ε = 80 for water (we neglect the cavitation energy contribution). We also assumed that the total quantities of energy and entropy of the translational and the rotational motion have been fully quenched in the solvated state, which means that only vibrational motions are effective in the solvated state. The partial density of states (PDOS) was calculated with the conditions of Gaussian smearing and a 0.01 eV broadening

dx.doi.org/10.1021/ja503782w | J. Am. Chem. Soc. 2014, 136, 11355–11361

parameter and was visualized with the visualization for electronic and structural analysis (VESTA) program.[18]

RESULTS AND DISCUSSION

Among various possible final products such as formic acid (HCOOH), carbon monoxide (CO), methanol (CH_3OH), ethylene (C_2H_4), and so forth,[19,20] we chose our target final product as CO. This is not merely because the production of CO requires the simplest electrochemical pathway (consuming only two electrons) so that the reaction pathways can be effectively controlled, as we designed in our simulations without involving complicated side reactions, but more importantly is because CO is a valuable product widely used in chemical industry such as the Fischer–Tropsch process, the Monsanto process, and so forth.

We further note that the domain of our target catalyst is limited to heterogeneous metal catalysts. When only the catalytic center is embedded in the electrode surface, the electron transfer from the electrode to the catalyst can be facile and less dependent on the electrolyte double layer characteristics, which can be beneficial in maximizing the overall catalytic efficiency. In addition, the use of heterogeneous catalysts has advantages for application to large-scale industry applications.

We consider three elementary reaction steps for the electrochemical reduction process from CO_2 to CO on a metal surface as shown in Figure 1a:[21]

1. The first electron-transfer step from the catalyst to CO_2, coupled with a simultaneous proton transfer from the electrolyte, yielding ·COOH that is immediately stabilized on the metal surface by forming a metal–carbon bond.
2. The second electron-transfer step from the catalyst to the adsorbed ·COOH (*COOH) on the metal surface, coupled with a simultaneous proton transfer from the electrolyte, yielding adsorbed CO (*CO) and releasing H_2O into the electrolyte.
3. A *CO-releasing step from the metal surface to the gas phase.

Here, the first two steps involve electrochemical reactions, whereas the third step does not, and we denote the thermodynamic energy change for each elementary step as $\Gamma_{1/2/3}$.

We then conceived hypothetical reaction pathways in which all chemical species are not adsorbed onto the metal surfaces but exist within the bulk electrolyte, for which the reaction free energies are denoted as $\Delta G_{1/2/3}$. Using the thermodynamic cycles shown in Figure 1a, we relate the free energies of catalyzed reactions, $\Gamma_{1/2/3}$, to the catalyst-free reaction free energies, $\Delta G_{1/2/3}$, by introducing binding free energies of ·COOH ($\Delta G_{B,COOH}$) and CO ($\Delta G_{B,CO}$) under the solvation conditions

$$\Gamma_1 = \Delta G_1 + \Delta G_{B,COOH} \quad (1.1)$$

$$\Gamma_2 = \Delta G_2 + \Delta G_{B,CO} - \Delta G_{B,COOH} \quad (1.2)$$

$$\Gamma_3 = \Delta G_3 - \Delta G_{B,CO} \quad (1.3)$$

We computed the vibrational frequencies using DFT calculations and the solvation free energies using DFT+PB, which we then used to yield $\Delta G_1 = 2.02$ eV, $\Delta G_2 = -1.07$ eV, and $\Delta G_3 = -0.50$ eV (Supporting Information Table S1). Because we used the chemical potential of a proton and an electron pair as the same value as the free energy of 1/2 H_2 (g), we can directly convert ΔG into reduction potential values (E°) vs the standard hydrogen electrode (SHE)[22] via the Nernst equation ($\Delta G = -nFE^\circ$; $n = 1$ and $F = 1$ when ΔG is given in eV). This suggests that the first reduction process (more unfavored than the second reduction step) is the source for the electrochemical overpotential, resulting in the reduction potential E° of −2.02 V vs SHE [= −MAX(2.02, −1.07)], for the noncatalyzed hypothetical process.

When the effect of the catalyst is considered, we can define the theoretical reduction potential (E°_{Theory}) as a function of $\Delta G_{B,COOH}$ and $\Delta G_{B,CO}$ as follows:

$$\begin{aligned} E^\circ_{Theory} &= -\mathrm{MAX}(\Gamma_1, \Gamma_2) \\ &= -\mathrm{MAX}(2.02 + \Delta G_{B,COOH}, -1.07 + \Delta G_{B,CO} \\ &\quad - \Delta G_{B,COOH}) \end{aligned} \quad (2)$$

To confirm this approach, we calculated $\Delta G_{B,COOH}$ and $\Delta G_{B,CO}$ for zinc (Zn), silver (Ag), and gold (Au), which are experimentally known to convert CO_2 into CO, using DFT-PB and vibrational frequency calculations (Supporting Information Table S1). We find that the E°_{Theory} values for these pure metals are remarkably consistent with the experimental reduction potentials ($E^\circ_{Experimental}$),[7] defined as the required potential for 5 mA cm^{-2} current density (Figure 1b). We further find that all Γ_3 values for Zn, Ag, and Au are negative, that is, they favor CO desorption, which infers that CO is produced as the final product without further reduction.

We additionally calculated E°_{Theory} for copper (Cu). Because CO desorption is not favorable on Cu ($\Gamma_3 = 0.37$ eV > 0), CO can experience further reductions to yield methanol, methane, and so forth by consuming six to eight or more electrons as observed from experiments.[23] Our calculations find that the source of the overpotential in the Cu case is the third reduction process when the adsorbed CO is reduced into either ·COH or ·CHO, in accordance with a previous theoretical study.[24] This alters the E°_{Theory} value for Cu to −0.97 V (vs SHE; Supporting Information Table S2), which is also in excellent agreement with $E^\circ_{Experiment} = -1.02$ V (vs SHE).

From eq 2, which is now validated against experimental values, we can display E°_{Theory} as a contour map for a range of $\Delta G_{B,COOH}$ and $\Delta G_{B,CO}$ (Figure 1c) values. Because we aim to design catalysts that produce CO, only the region where CO desorption is favored ($\Gamma_3 < 0$, i.e., $\Delta G_{B,CO} > -0.5$ eV) is in our interest. The trend of E°_{Theory} shows volcano-type behavior for the given $\Delta G_{B,COOH}$. As ·COOH becomes more stabilized on the metal surface, the potential required for the first reduction step (Γ_1) is linearly decreased; however, this simultaneously increases the potential required for the second reduction step (Γ_2), which eventually invert the source of the overpotential from the first to the second reduction step after a minimum (i.e., the apex of the activity volcano). This leads to a local minimum line of E°_{Theory} along the condition of $\Gamma_1 = \Gamma_2$, for which the minimum E°_{Theory} (minimum theoretical bound) is −0.22 eV and $\Delta G_{B,COOH} = -1.80$ eV and $\Delta G_{B,CO} = -0.5$ eV.

The stabilization effects by the pure metal for ·COOH and CO are strongly correlated, leading to a linear correlation line between $\Delta G_{B,COOH}$ and $\Delta G_{B,CO}$, which is shifted from the minimum reduction potential line of $\Gamma_1 = \Gamma_2$ (Figure 1c). The mismatch of the $\Delta G_{B,CO}$–$\Delta G_{B,COOH}$ correlation line and the minimum reduction potential line gives us a region for optimizing catalysts to minimize the thermodynamic barrier

dx.doi.org/10.1021/ja503782w | J. Am. Chem. Soc. 2014, 136, 11355–11361

by variously modifying the binding characteristics of ·COOH and CO and thereby disrupting the correlation between $\Delta G_{B,COOH}$ and $\Delta G_{B,CO}$ for pure metallic systems.

We consider that the low concentration of doping on a pure metal surface, yielding a heterogeneous atom embedded within the metal, can provide a good active site for CO_2 reduction. It is expected to modulate the binding characteristics of ·COOH and CO by changing the electronic structure in the vicinity of the adsorbents. In our high-throughput screening process, we therefore substitute one metal atom at the surface with various types of dopant metals, metalloids, nonmetals, and halogen species (Figure 2). As the base metal, we selected Ag due to its

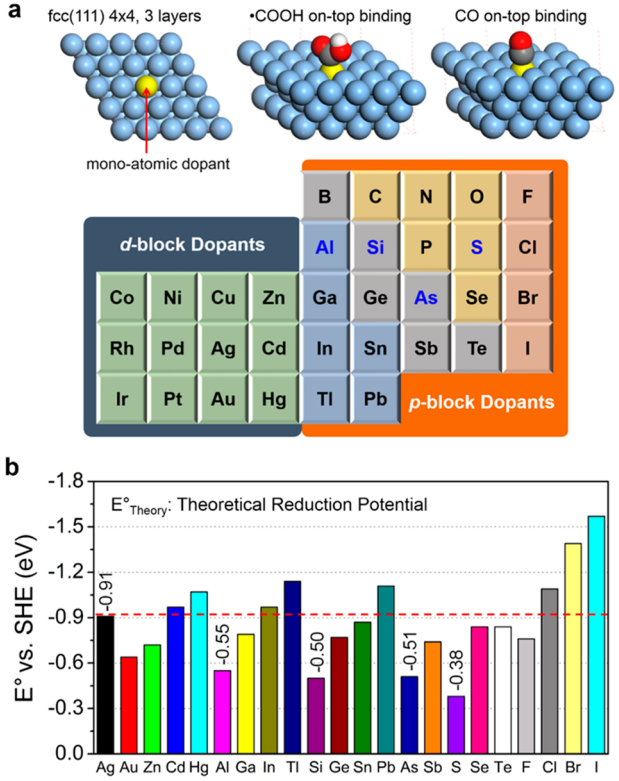

Figure 2. High-throughput screening strategy and a summary of the result. (a) Structural models for high-throughput screening and the list of dopants that can be categorized as *d*-block and *p*-block atoms. A monatomic dopant is substituted for one silver (Ag) atom on the top layer. The binding energies of ·COOH and CO on the dopant atop site. (b) Summary of the theoretical reduction potential for dopants for which $\Delta G_{B,CO} > -0.5$ eV. More refined calculations (in-depth binding site search and high-precision binding energy calculation) have been conducted for the best four candidates, S, As, Si, and Al, resulting in $E^{\circ}_{Theory} = -0.38$ V (S), −0.51 V (As), −0.50 V (Si), and −0.55 V (Al) vs SHE.

potential reactivity and stability,[25] which overcomes the problems known for other metals, including: (1) Cu has a significant activity-degradation problem,[26] (2) Au is a precious metal, and (3) Zn has insufficiently low activity. For a pure Ag system, because the first reduction step is the source of the overpotential ($\Gamma_1 > \Gamma_2$), we must design dopants that can moderately stabilize ·COOH (reducing Γ_1) with the smallest stabilizing effect (or even with a destabilizing effect) on CO to maintain favorable CO desorption and avoid much of an increase in Γ_2. For fast screening, we omitted the time-consuming frequency calculations for the direct evaluation of the vibrational entropic contributions. We instead calculated and used the binding energies of ·COOH and CO in the gas phase ($\Delta E_{B,COOH}$ and $\Delta E_{B,CO}$) for on-top site for a dopant atom, which was linearly scaled to predict the binding free energy under solvation ($\Delta G_{B,COOH}$, $\Delta G_{B,CO}$) using the linear correlation between ΔE_B and ΔG_B (Supporting Information Figure S1).

For the transition-metal dopants (namely, *d*-block dopants), we find that there still exists a strong correlation between $\Delta G_{B,COOH}$ and $\Delta G_{B,CO}$, as shown in Figure 3a, which provides little room for optimization and results in an activity range similar to that of the pure metallic catalysts.[24] This is not surprising because the binding energy of an adsorbent on *d*-metals is often well described by a single metric called a *d*-band center.[27] In our systems with *d*-block dopants, partially filled and delocalized *d*-bands are utilized to form a bond either with · COOH or CO, and therefore, it is possible to correlate $\Delta G_{B,COOH}$ and $\Delta G_{B,CO}$ with the location of the *d*-band center (Figure 3b). Because the modulation of the *d*-band center modifies $\Delta G_{B,COOH}$ and $\Delta G_{B,CO}$ simultaneously, the preferred stabilization of ·COOH over CO is rarely achievable using *d*-block elements, which is an intrinsic limit of *d*-block dopants or metallic alloys for CO_2-to-CO conversion technology. We note that the values for the metal dopants of group 11 and 12 deviate slightly from the correlation between the *d*-band center and the binding energies, possibly due to their fully occupied valence *d*-orbitals ($d^{10}s^1$ for group 11 and $d^{10}s^2$ for group 12). However, this effect is not large enough to alter the previous argument.

For *p*-block dopants, however, we observe a weakened correlation between $\Delta G_{B,COOH}$ and $\Delta G_{B,CO}$ (Figure 3c); as a result, certain dopants, such as sulfur, lead to a minimized E°_{Theory} of −0.39 V (only 0.17 V higher than the theoretical minimum bound). The location of the *d*-band center of Ag with *p*-block dopants cannot explain the trend of $\Delta G_{B,COOH}$ and $\Delta G_{B,CO}$ (Figure 3d), indicating that a new mechanistic rationale for *p*-block dopants is necessary.

When ·COOH binds to *p*-block elements, a singly occupied p_z orbital, $(p_z)^1$ can stabilize the radical electron localized in the $2p_z$ orbital of C in ·COOH. Considering that the *p*-orbitals of the dopant atom are highly hybridized with the *d*-band of the host Ag metal when no absorbent exists (Supporting Information Figure S2), an additional energy cost is required to spatially localize the singly occupied p_z orbital (i.e., a radical) of the dopant atom to prepare $(p_z)^1$ (Figure 4a). Thus, we decompose $\Delta G_{B,COOH}$ into two components, (1) a radical-preparation energy cost (E_{rp}) and (2) a covalent-bond-stabilization energy ($E_{\sigma\text{-bond}}$) due to the σ-bond between $(p_z)^1$ of the dopant atom and $(2p_z)^1$ of ·COOH. We then quantified the ΔE_{rp} value using the difference of the D-H homolytic bond dissociation energy when the dopant atom (D) is fully hydrogenated (DH_n) and that when D is embedded in Ag: $E_{rp} = BE(H_{n-1}D—H) - BE(AgD—H)$, where BE is the bond energy (Figure 4b). $E_{\sigma\text{-bond}}$ is quantified as the bond energy of ($H_{n-1}D—COOH$) for which the pure σ-bond is between the prepared radical on the dopant and ·COOH (Figure 4c). The difference between the E_{rp} and $E_{\sigma\text{-bond}}$ ($E_{rp} - E_{\sigma\text{-bond}}$) values agrees well with the direct calculation of $\Delta E_{B,COOH}$ (Supporting Information Figure S3), implying that our two-component decomposition of $\Delta E_{B,COOH}$ is reasonable. The slight mismatches in the cases of B, C, N, and O are presumably due to the strong *s*−*p* hybridization character of the second-row elements.

dx.doi.org/10.1021/ja503782w | J. Am. Chem. Soc. 2014, 136, 11355−11361

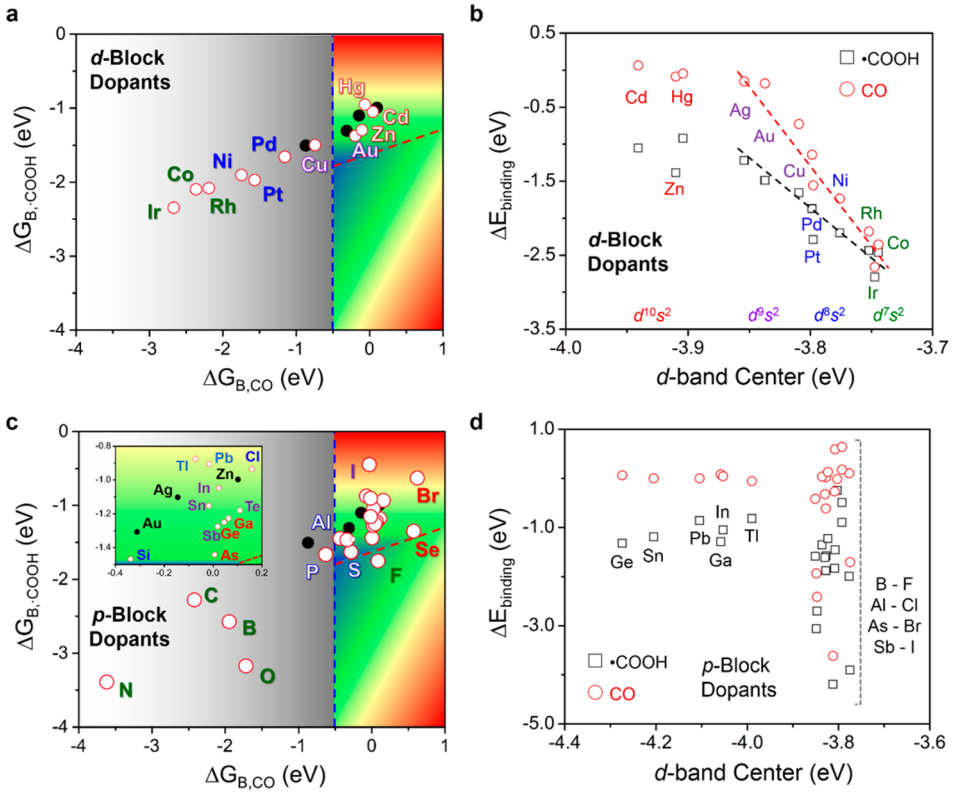

Figure 3. Variations of ·COOH and CO stabilization depending on the dopants and their correlation with the *d*-band center. (a) ·COOH and CO binding free energies, $\Delta G_{B,\cdot COOH}$ and $\Delta G_{B,CO}$, of the *d*-block dopants. A linear correlation between $\Delta G_{B,\cdot COOH}$ and $\Delta G_{B,CO}$ is conserved, similar to the case of pure metals. (b) Correlation between the locations of the *d*-band center and the binding energies for *d*-block dopants. This shows that dopants modulate the locations of the *d*-band center of Ag catalysts, resulting in a similar magnitude of modulations in $\Delta G_{B,\cdot COOH}$ and $\Delta G_{B,CO}$, maintaining the strong intercorrelation between $\Delta G_{B,\cdot COOH}$ and $\Delta G_{B,CO}$. (c) $\Delta G_{B,\cdot COOH}$ and $\Delta G_{B,CO}$ of the *p*-block dopants. Variations in the binding characters are much greater than those of *d*-block dopants and, therefore, the minimum theoretical bound of −0.22 eV is nearly achievable with sulfur. (d) Correlation between the locations of the *d*-band center and the binding energies for *p*-block dopants. Almost no correlation is observed, implying that the covalency-aided electrochemical reaction (CAER) mechanism is required for the explanation of the wide variations in $\Delta G_{B,\cdot COOH}$ and $\Delta G_{B,CO}$ caused by the *p*-block dopants that are not consistent with *d*-band center theory.

We find that E_{rp} has a strong column dependency. Particularly, the halogen column has a highly unfavored E_{rp}. Due to the high electronegativity, these dopant atoms are negatively charged (see the Bader charge analysis in Supporting Information Table S3). Thus, the electronic configuration of the halogen dopants can be conceived as $p^{5.x}$, where all six *p* orbitals (considering spin degeneracy) are either fully or at least partly occupied. This results in a high energy cost to vacate the p_z orbital.

For the trend of $E_{\sigma\text{-bond}}$, we observe a strong row dependency, that is, for the principal quantum number (n) of the valence *p* orbital of the dopant atom. This can be rationalized easily by using the relative location of the np_z orbital of the dopant atoms with respect to the location of the $2p_z$ orbital of C in ·COOH, resulting in the strongest $E_{\sigma\text{-bond}}$ for the closest cases for which $n = 2$ and a tendency that weakens as the row goes down.

The σ-binding mechanism of CO is different from that of ·COOH, for which the lone pair electrons of C in CO are coordinated to the dopant atom; therefore, an empty p_z orbital is required at the dopant site, $(p_z)^0$, and a more significant energy-consuming process is required to entirely vacate the p_z orbital. We thus find that the CO binding to the halogen group dopants ($p^{5.x}$) is significantly unstable, requiring the emptying of the *1.x* electrons, and the binding to the oxygen group dopants ($p^{4.x}$) is also unstable, requiring the emptying of the *0.x* electrons (Supporting Information Table S3).

Regarding all of these factors, the dopant sulfur yields the most appropriate $\Delta G_{B,COOH}$ and $\Delta G_{B,CO}$ regimes, yielding $E^{\circ}_{Theory} = -0.39$ eV; it has a weak binding energy with CO as an oxygen-group element, but it has a moderately strong binding energy with ·COOH as a nonhalogen and a third-row element. Essentially, this type of selective stabilization of ·COOH over CO is enabled due to the covalent character imposed on the Ag metal catalysts, originating from the localized *p* orbital of the dopant element, which can be referred to as a covalency-aided electrochemical reaction (CAER) mechanism. We additionally find that aluminum, silicon, and arsenic are good candidate dopants for use in the CAER mechanism to minimize the overpotential ($E^{\circ}_{Theory} = -0.57$, −0.55, and −0.58 V, respectively).

From more in-depth calculations on the S-dopant system for various adsorption sites, we find that the on-top site provides the strongest binding to ·COOH, whereas the 3-fold FCC site provides the strongest binding for CO (Supporting Information Figure S4). It should be further noted that the binding energy is almost fully recovered to that of the pure Ag surface from the on-top site of the Ag atom nearest to the dopant S atom, indicating that the range of the dopant effect on the binding energy is very local. Using accurate free-energy calculations (from direct frequency calculations) based on the correct

dx.doi.org/10.1021/ja503782w | J. Am. Chem. Soc. 2014, 136, 11355−11361

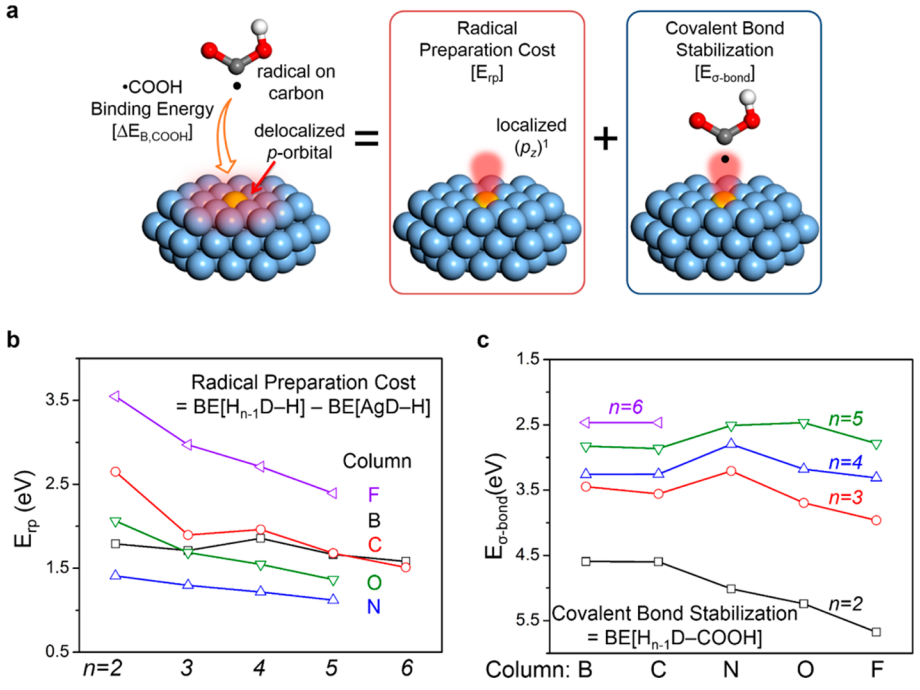

Figure 4. Rationalization of the CAER mechanism. (a) Schematic diagram of the ·COOH binding mechanism on *p*-block dopants. It first necessitates preparing a singly occupied p_z orbital on the dopant atom by localizing the orbital (Supporting Information Figure S2) (energy-consuming step), and then forming a covalent bond between the prepared $(p_z)^1$ of the dopant atom and the $(2p_z)^1$ of ·COOH (energy-stabilizing step). (b) The row dependency (i.e., the principal quantum number (n) of the valence p orbital of the dopant atom) of the radical-preparation cost (c) The column dependency of the covalent bond stabilization energy.

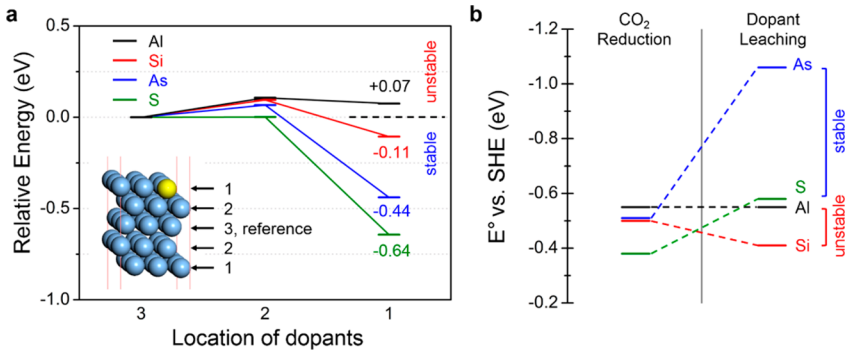

Figure 5. Structural and electrochemical stability of the dopants. (a) Energetically preferential sites of dopant atoms (S, As, Si, and Al) from the subsurface to the outermost surface. S, As, and Si prefer to remain on the surface whereas Al prefers to diffuse into the sublayers. (b) Comparison between the theoretical reduction potentials ($E°$) for CO_2-to-CO reduction and leaching of the dopant atom to hydride form such as AlH_3, SiH_4, AsH_3, and H_2S. For As and S, $E°$ for dopant leaching is higher than $E°$ for CO_2 reduction, preserving the electrochemical stability of the dopant atoms.

binding sites, we refined $E°_{Theory}$ for an S dopant, leading to the change of a more energy-consuming step from the first reduction step to the second step, but retaining $E°_{Theory}$ at almost the same value of −0.38 V (Γ_1 = 0.26 eV, Γ_2 = 0.38 eV). In a similar manner, the refined $E°_{Theory}$ for Si, Al, and As are −0.50 V, −0.55 V, and −0.51 V, respectively (Figure 2b).

We further investigated the stability of surface dopant atoms from the sublayer diffusion process. Within a (3 × 3) five-layer Ag FCC (111) slab model, S, Si, and As preferentially locate on the outer layer by 0.11−0.64 eV, whereas Al preferentially migrates into the sublayers, stabilized by −0.07 eV (Figure 5a). Furthermore, we find that the required potentials for leaching the dopant atoms by an electrochemical hydrogenation reaction are −0.58 V (S), −0.41 V (Si), −0.55 V (Al), and −1.06 V (As) vs SHE, which provide the upper bounds of the operating potential with stable dopants. For Al and Si, $E°_{Theory}$ for CO_2 reduction is similar to, or even higher than, the upper bound, resulting in a stability problem. However, for S and As, $E°_{Theory}$ for CO_2 reduction is located below the dopant-leaching potential (Figure 5b).

CONCLUSION

Considering the structural and electrochemical stabilities, we anticipate that the realization of Ag-based catalysts doped by S or As can be experimentally achieved, leading to a markedly reduced overpotential by 0.4−0.5 V for efficient CO_2-to-CO electrochemical conversion. Moreover, we provide a new design principle, the CAER mechanism, in which specific stabilization of intermediates can be achieved by utilizing *p*-block elements to move beyond *d*-band-center engineering. This illustrates

dx.doi.org/10.1021/ja503782w | J. Am. Chem. Soc. 2014, 136, 11355−11361

how new first-principles-based high-throughput screening can suggest new designs for electrochemical catalysts to achieve new technologies, such as the carbon dioxide (CO_2) conversion technology.

■ ASSOCIATED CONTENT

Supporting Information

Detailed information regarding quantum mechanical thermodynamic data, partial charge analysis, and supportive figures. This material is available free of charge via the Internet at http://pubs.acs.org.

■ AUTHOR INFORMATION

Corresponding Author

linus16@kaist.ac.kr

Author Contributions

[§]These authors contributed equally.

Notes

The authors declare no competing financial interest.

■ ACKNOWLEDGMENTS

This work was supported by the Global Frontier R&D Program (2013M3A6B1078884) on Center for Hybrid Interface Materials (HIM) funded by the Ministry of Science, ICT & Future Planning, and by the institutional program of the Korea Institute of Science and Technology (KIST). We also acknowledge the Supercomputing Center/Korea Institute of Science and Technology Information with supercomputing resources including technical support (KSC-2013-G3-002).

■ REFERENCES

(1) Roy, S. C.; Varghese, O. K.; Paulose, M.; Grimes, C. A. *ACS Nano* **2010**, *4*, 1259.

(2) Saveant, J. M. *Chem. Rev.* **2008**, *108*, 2348.

(3) Whipple, D. T.; Kenis, P. J. A. *J. Phys. Chem. Lett.* **2010**, *1*, 3451.

(4) Keene, F. R. In *Electrochemical and Electrocatalytic Reactions of Carbon Dioxide*; Sullivan, B. P., Ed.; Elsevier: Amsterdam, 1993; p 1.

(5) Lamy, E.; Nadjo, L.; Saveant, J. M. *J. Electroanal. Chem.* **1977**, *78*, 403.

(6) Benson, E. E.; Kubiak, C. P.; Sathrum, A. J.; Smieja, J. M. *Chem. Soc. Rev.* **2009**, *38*, 89.

(7) Hori, Y.; Wakebe, H.; Tsukamoto, T.; Koga, O. *Electrochim. Acta* **1994**, *39*, 1833.

(8) Curtarolo, S.; Hart, G. L. W.; Nardelli, M. B.; Mingo, N.; Sanvito, S.; Levy, O. *Nat. Mater.* **2013**, *12*, 191.

(9) Hautier, G.; Jain, A.; Chen, H. L.; Moore, C.; Ong, S. P.; Ceder, G. *J. Mater. Chem.* **2011**, *21*, 17147.

(10) Hautier, G.; Jain, A.; Ong, S. P.; Kang, B.; Moore, C.; Doe, R.; Ceder, G. *Chem. Mater.* **2011**, *23*, 3495.

(11) Ceder, G. *MRS Bull.* **2010**, *35*, 693.

(12) Greeley, J.; Jaramillo, T. F.; Bonde, J.; Chorkendorff, I. B.; Norskov, J. K. *Nat. Mater.* **2006**, *5*, 909.

(13) Yu, L. P.; Zunger, A. *Phys. Rev. Lett.* **2012**, *108*, 068701.

(14) Wilmer, C. E.; Leaf, M.; Lee, C. Y.; Farha, O. K.; Hauser, B. G.; Hupp, J. T.; Snurr, R. Q. *Nat. Chem.* **2012**, *4*, 83.

(15) Kresse, G.; Furthmuller, J. *Phys. Rev. B* **1996**, *54*, 11169.

(16) Perdew, J. P.; Burke, K.; Ernzerhof, M. *Phys. Rev. Lett.* **1996**, *77*, 3865.

(17) Fishman, M.; Zhuang, H. L. L.; Mathew, K.; Dirschka, W.; Hennig, R. G. *Phys. Rev. B* **2013**, *87*, 245402.

(18) Momma, K.; Izumi, F. *J. Appl. Crystallogr.* **2011**, *44*, 1272.

(19) Azuma, M.; Hashimoto, K.; Hiramoto, M.; Watanabe, M.; Sakata, T. *J. Electrochem. Soc.* **1990**, *137*, 1772.

(20) Kuhl, K. P.; Cave, E. R.; Abram, D. N.; Jaramillo, T. F. *Energ Environ. Sci.* **2012**, *5*, 7050.

(21) Hansen, H. A.; Varley, J. B.; Peterson, A. A.; Norskov, J. K. *J. Phys. Chem. Lett.* **2013**, *4*, 388.

(22) Norskov, J. K.; Rossmeisl, J.; Logadottir, A.; Lindqvist, L.; Kitchin, J. R.; Bligaard, T.; Jonsson, H. *J. Phys. Chem. B* **2004**, *108*, 17886.

(23) Hori, Y.; Murata, A.; Takahashi, R. *J. Chem. Soc., Faraday Trans. 1* **1989**, *85*, 2309.

(24) Peterson, A. A.; Norskov, J. K. *J. Phys. Chem. Lett.* **2012**, *3*, 251.

(25) Rosen, B. A.; Salehi-Khojin, A.; Thorson, M. R.; Zhu, W.; Whipple, D. T.; Kenis, P. J. A.; Masel, R. I. *Science* **2011**, *334*, 643.

(26) Hori, Y.; Konishi, H.; Futamura, T.; Murata, A.; Koga, O.; Sakurai, H.; Oguma, K. *Electrochim. Acta* **2005**, *50*, 5354.

(27) Hammer, B.; Norskov, J. K. *Surf. Sci.* **1995**, *343*, 211.